Journal of Marine Research, 64, 43–71, 2006

Understanding the influence of Rossby waves on surface chlorophyll concentrations in the North Atlantic Ocean

by G. Charria[1,2], I. Dadou[1], P. Cipollini[3], M. Drévillon[4], P. De Mey[1] and V. Garçon[1]

ABSTRACT

The variability (in space and time) of westward propagating Rossby waves is analyzed with a wavelet method between 10N and 40N in the North Atlantic Ocean using two remotely sensed data sets (Sea Level Anomalies – SLA and surface chlorophyll-*a* concentrations) in order to better understand the waves' characteristics and their impacts on the chlorophyll distribution. Signals with wavelengths between ~ 500 km and ~ 1000 km with ~ 4- to ~ 24-month periods were detected and identified as the first baroclinic mode of Rossby waves. The spatial and temporal information has also highlighted a particular situation in 1998 at 34N, with the simultaneous existence of two distinct wave components corresponding to wavelengths 500 km *and* 1000 km.

Signatures of the waves in ocean color prompt the question of how Rossby waves influence surface chlorophyll concentrations. Several physical/biological processes have been suggested: the eddy pumping mechanism associated with nutrient injection, the uplifting of a deep chlorophyll maximum toward the surface, and the meridional advection of horizontal chlorophyll gradients by geostrophic currents associated with baroclinic Rossby waves. A statistical decomposition of the observed signal into the different processes modeled by Killworth *et al.* (2004) confirms a main contribution of the north-south advection of the surface chlorophyll-*a* gradients south of 28N. In this part of the basin, more than ~ 70% of the signal is explained by this horizontal process. North of 28N, Rossby wave signatures seem to be due to the horizontal advection as well as the vertical nutrient injection (~ 50% of the observed amplitude). This vertical mechanism may have an impact on the primary production in this part of the basin.

1. Introduction

Rossby waves (also known as planetary waves) play an important role in the dynamics of the oceans. The westward propagating potential energy helps to maintain the mid-latitude gyres and to intensify the western boundary currents (Polito and Liu, 2003). Oceanic Rossby waves were for first observed in the 1970s and 1980s using XBT data (see Fu and Chelton, 2001, for a full review of the *in situ* observations). *In situ* measurements are not enough to fully describe and understand these waves due to their sparse spatial and

1. Laboratoire d'Etudes en Géophysique et Océanographie Spatiales, Centre National de la Recherche Scientifique, 18 Avenue Edouard Belin, 31401 Toulouse Cedex 9, France.
2. Corresponding author. ***email: guillaume.charria@notos.cst.cnes.fr***
3. National Oceanography Centre, European Way, Southampton SO14 3ZH, United Kingdom.
4. CERFACS, 42 Avenue G. Coriolis, 31057 Toulouse, Cedex, France.

temporal coverage. Nevertheless, the numerical simulations following these observations allowed the first studies of the properties of these waves. With the development of satellite measurements, it finally became possible to observe Rossby waves in the form of westward-propagating features in time/longitude diagrams of Sea Level Anomalies (SLA) from radar altimeters (e.g.: Chelton and Schlax, 1996; Cipollini *et al.*, 1997; Polito and Liu, 2003; Fu, 2004) as well as in Sea Surface Temperature (SST) from infrared sensors (e.g.: Cipollini *et al.*, 1997; Hill *et al.*, 2000).

Recently, a number of papers have described features associated with planetary waves in ocean color data (chlorophyll-*a* concentration) (e.g.: Machu *et al.*, 1999; Cipollini *et al.,* 2001; Uz *et al.*, 2001; Kawamiya and Oschlies, 2001). The observations of such signals prompt the question of how Rossby waves influence surface chlorophyll concentrations. Several physical/biological processes which might be involved have been suggested: (1) the eddy pumping mechanism associated with nutrient injection (Cipollini *et al.*, 2001; Uz *et al.*, 2001; Siegel, 2001), (2) the uplifting of a deep chlorophyll maximum toward the surface (Cipollini *et al.*, 2001; Kawamiya and Oschlies, 2001; Charria *et al.*, 2003), and (3) the meridional advection of horizontal chlorophyll gradients by geostrophic currents associated with baroclinic Rossby waves (Killworth *et al.*, 2004). These different processes are described using theoretical models and are compared to the remotely sensed observations in a recent paper by Killworth *et al.* (2004). A fourth process, the accumulation of phytoplankton detritus in convergent zones as the waves pass, was also suggested (Dandonneau *et al.*, 2003), but its occurrence is still subject of debate (Killworth, 2004; Dandonneau *et al.*, 2004).

This paper aims at (a) investigating the spatial and temporal variability of Rossby waves and their effects on chlorophyll-*a* concentrations in the North Atlantic between 10N and 40N and (b) quantifying the relative importance of the different physical/biological processes over the same region. This part of the Atlantic Ocean includes very different biogeochemical provinces (Longhurst, 1998) and is characterized by a strong phytoplankton spring bloom inducing a well-marked chlorophyll frontal zone. Furthermore, an oligotrophic area, due to the existence of the subtropical gyre, resides south of 30N. This spatial variability allows us to analyze the influence of Rossby waves in the presence of very different background chlorophyll conditions.

The work is divided in two parts. In the first part of the study (Section 2), we characterize the variability in space and time of Rossby waves in two simultaneous remotely sensed data sets (Sea Level Anomalies and Chlorophyll-*a* concentrations) in the North Atlantic Ocean, using a wavelet transform approach. Previous studies had not analyzed the temporal variability (with the exception of Cromwell (2001) at the single latitude of 34N on SLA only). Using two data sets allows us a first step into assessing the likelihood of the different mechanisms by which planetary waves may affect the signal we observe in ocean color and allows location in time and/or space of any anomalous conditions that may deserve further study.

In the second part of the study (Section 3), process modeling from Killworth *et al.*

(2004) is compared with result of a cross-spectral wavelet analysis of SLA and chlorophyll in order to investigate the interplay of the three aforementioned coupled biological/physical mechanisms over the same area. As it will be shown in the following, this study broadly confirms the findings by Killworth *et al*. (2004) and gives additional information on the temporal variability of the SLA/chlorophyll relationship. Nevertheless, over part of the basin this analysis is not sufficient to remove the ambiguity in attributing the signals observed in ocean color to one or the other mechanism. Therefore, we finally attempt a quantitative decomposition of the observed relationship between SLA and ocean color based on statistical argumentations to estimate the share of the signal due to each process.

2. Rossby wave features in the North Atlantic

a. Remotely sensed data

i. Chlorophyll-a concentrations. Chlorophyll-*a* concentrations (in mg m^{-3}) were obtained from the ocean color sensor SeaWiFS (Sea-viewing Wide Field-of-view Sensor) products (level 3 binned data, monthly, version 4 - O'Reilly *et al.*, 1998) generated by the NASA Goddard Space Flight Center (GSFC) Distributed Active Archive Center (DAAC) (McClain *et al.*, 1998). We used the products on a regular grid of 9 by 9 km from January 1998 to December 2001. The predicted error on the single 1-km SeaWiFS estimates of chlorophyll-*a* concentration is 35 % (McClain *et al.*, 1998); the accuracy of 9 km gridded data is comparable or better. As our study focuses on the anomalies of chlorophyll-*a* concentrations, we remove a monthly zonal average from raw data at each latitude and for each month. To apply the spectral wavelet analysis described below, the residual gaps in the data, mainly due to the presence of clouds, are filled with a linear interpolation.

ii. Sea Level Anomalies (SLA). Sea Level Anomaly data are provided by CLS Space Oceanography Division as part of the Environment and Climate EC AGORA and DUACS projects. These SLA were obtained from the combined processing of the Topex/Poseidon (T/P) and ERS-1/2 data. The two data sets were combined using an improved space/time objective analysis method taking into account long wavelength errors which correlated noise with a 1-2 cm mean error (Le Traon *et al.*, 1998). SLA are relative to a seven-year average (1993-1999) and were mapped every 7 days from October 1992 to February 2002 with a spatial resolution of 1/3°. To have the same temporal resolution as for the surface chlorophyll-*a* concentrations, SLA data were averaged with a monthly time step.

b. Methodology

In order to describe the spatial and temporal characteristics of Rossby waves in the North Atlantic from 10N to 40N, we adopt a spectral analysis method based on the Wavelet Transform (WT – see details in Appendix) (Torrence and Compo, 1998). We apply the WT in two different ways. A *spatial* wavelet analysis is carried out by applying the WT to zonal (east-west) sections of data at a given time step, and helps identify wavelength variability

in space along the section. A *temporal* wavelet analysis is carried out by applying the WT to a time series of data at a given location, and helps locate periods in time. Several studies have been performed with this spectral analysis tool on satellite data sets to study particular physical or biogeochemical processes. For example, Machu and Garçon (2001) and Charria *et al.* (2003) used this method to describe SeaWiFS ocean color data in the Agulhas Current system and in the South Atlantic, respectively, and Cromwell (2001) analyzed Topex/Poseidon altimetry data at 34N in the North Atlantic. In the present study, we first apply the WT to both data sets to study Rossby wave variability both in space (east of, west of and above the ridge) and in time (seasonal and inter-annual variability) in the North Atlantic Ocean. Subsequently, a cross-spectral analysis is performed to study the relationship between the SLA and the chlorophyll-*a* concentrations by computing (cross-)wavelet coherency and phase (Torrence and Webster, 1999). This method allows extracting coherency and phase for each scale (period or wavelength, for a temporal or a spatial analysis, respectively) at a given point in the case of a temporal wavelet analysis or at a given latitude and a particular date in the case of a spatial wavelet analysis (see details in Appendix). Due to the limited length of the time series of remotely sensed data sets (only 4 simultaneous years for the SLA and chlorophyll-*a* concentrations), the spatial cross-wavelet analysis will be used in preference to the temporal analysis.

c. Detection of Rossby waves in the North Atlantic Ocean: Results

i. Westward propagation observed on SLA. Westward propagating signals, previously identified by several authors as baroclinic Rossby waves due to their dynamical features (see Fu and Chelton, 2001, for a review), are clearly observed in time-longitude plots of SLA at all latitudes studied between 10N and 40N. Three examples are shown in Figure 1. Some pre-processing may be applied to highlight the signature of the waves; for visual analysis purposes we have reconstructed, with a 1D wavelet filtering, the signal between $j = 20$ and $j = 24$ (equivalent to wavelengths between 500 km and 1000 km) at each latitude. The choice of this wavelength range allows filtering out mesoscale signals. The features become clearer after filtering, as illustrated by the comparison of Figures 2a and b. The observed amplitude of the westward-propagating signals varies greatly with latitude, being larger at around 34N (Figs. 1 and 2). This feature could be due to the "waveguide effect," which in turn may be related to the interaction between the Azores zonal current and Rossby waves (Cipollini *et al*., 1997), in analogy with what happens in the Antarctic Circumpolar Current (Hughes, 1996). We also observe different behaviors as far as the longitudinal variability is concerned: at 20N the waves maintain roughly the same amplitude across the basin, whereas at 34N they are larger above the mid-Atlantic ridge and at 40N show a very strong amplification west of 40W, probably due to broadband energy associated with the Gulf Stream and/or to wave/current interaction.

ii. Spatial and temporal properties from SLA. To assess the spatial variability of Rossby waves, we applied a 1D spatial wavelet analysis to the unfiltered SLA. The analysis was

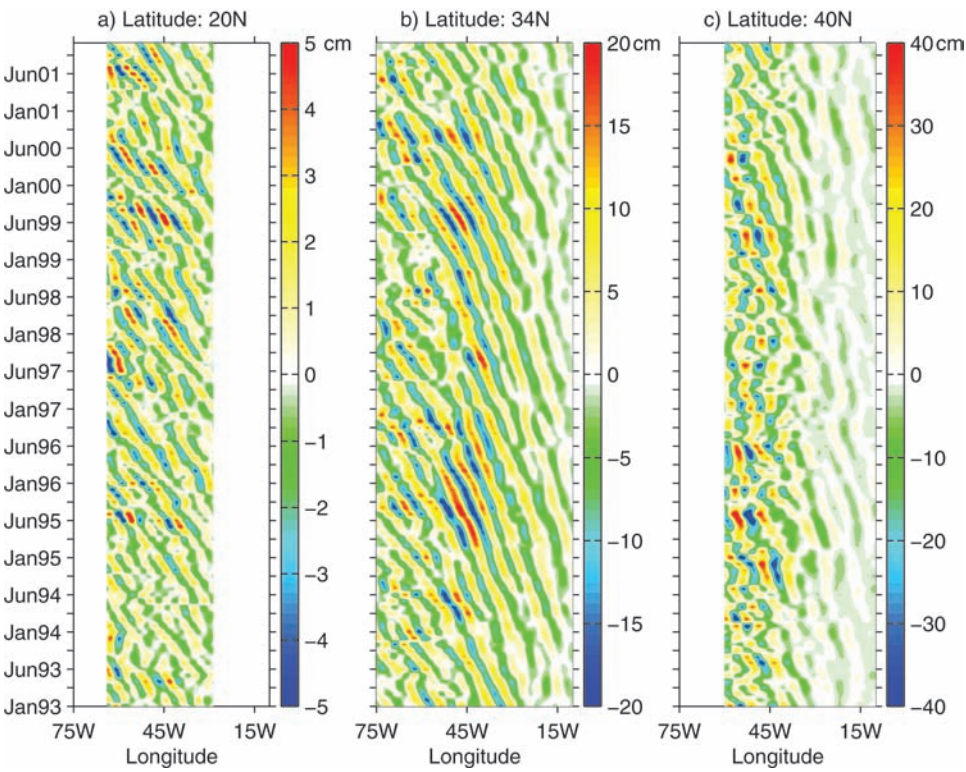

Figure 1. Time/longitude plots of SLA (cm) at (a) 20N, (b) 34N and (c) 40N. Data have been spatially filtered. Signals are reconstructed for wavelengths between 500 and 1000 km using a wavelet analysis.

performed month by month on sections spanning the whole zonal extent of the basin at each latitude value from 10N to 40N in 1° steps. The variable length of each section (more or less centered on the mid-Atlantic ridge where Rossby waves may be amplified (as discussed by Cromwell, 2001)) directly influences the values of the wavelengths that we could detect, delimited by the cone of influence on the local wavelet power spectrum (Fig. 3).

The results of this first part of the analysis highlight a strong latitudinal variability of the signal. There are usually maxima for wavelengths between ~ 500 km and ~ 1000 km associated to the westward propagations. As shown on Figure 3a, which presents an example for April 1998 at the latitude 34N, the maximum of wavelet coefficients (contoured by a black line indicating the 95% confidence level determined with a χ^2 test) is almost split into two wavelength bands at around ~500 km and ~1000 km, in the central part of the basin (these results agree with the findings of a 2D longitude/time Fourier transform and a 2D - latitude/longitude - Fourier transform combined with a 1D Gabor analysis in time - Pottier *et al.*, 2004). These two distinct wavelengths are not detected at

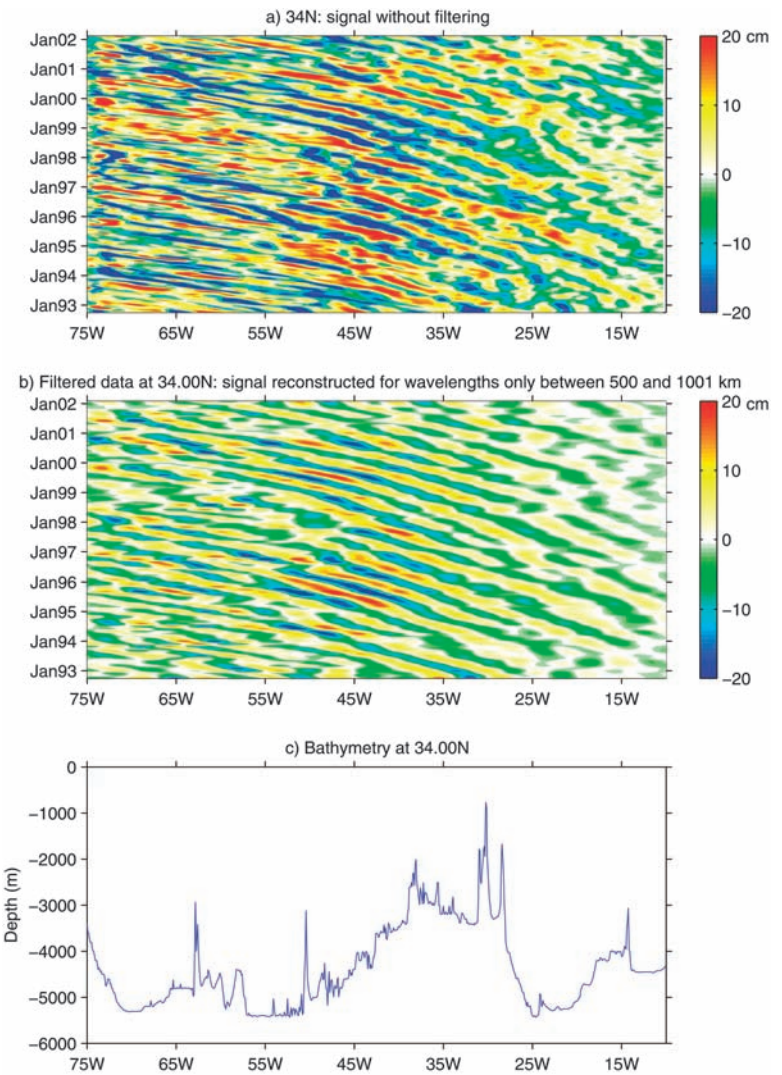

Figure 2. Time/longitude plots of SLA (cm) at 34N (a) signal without filtering and (b) signal is reconstructed for wavelengths only between 500 and 1000 km using a wavelet analysis and represent the filtered data. (c) Bathymetry at 34N.

28N where a broad maximum is observed from 500 to 700 km (Fig. 3b). From the analysis at all latitudes, it appears that a partition of energy into two distinct wavelengths only exists near 34N. Then we investigated whether such a peculiar partition of the signal is stationary or whether it only occurs at some specific times. By repeating the analysis for each month in the time series we observed that the double-wavelength configuration is most pronounced throughout almost all of 1998, except in some particular months (August and

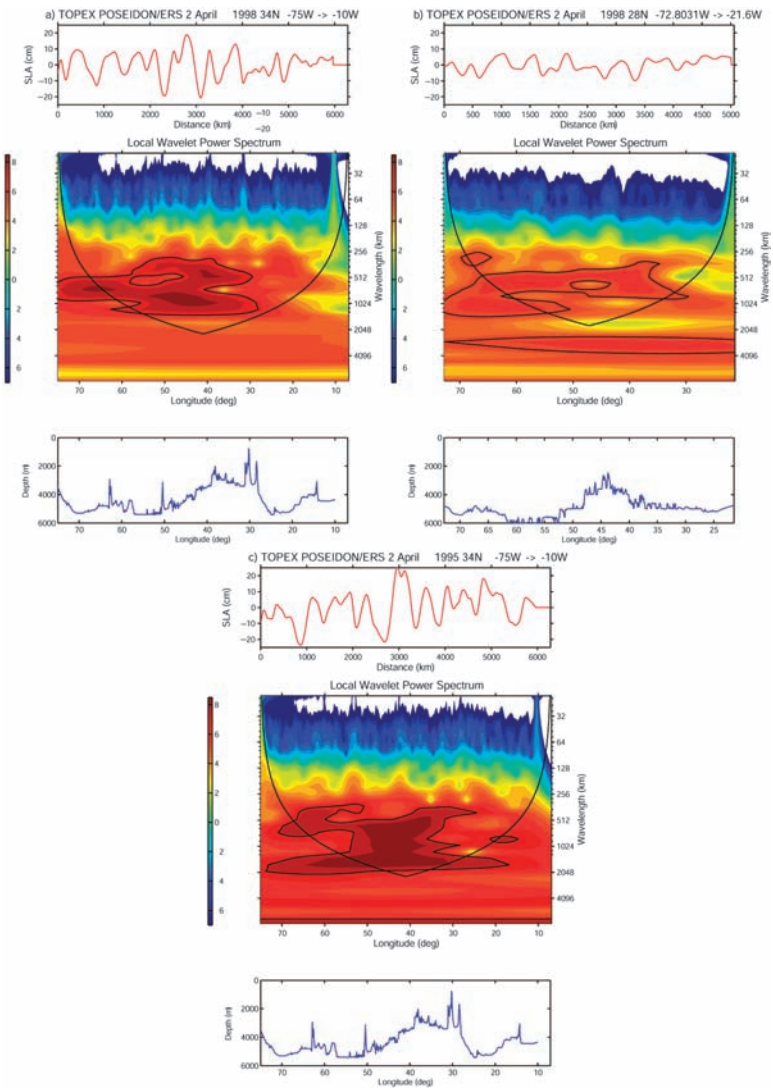

Figure 3. Spatial LWPS (Local Wavelet Power Spectrum) (a) at 34N for April 1998, (b) at 28N for April 1998, and (c) at 34N for April 1995. For (a), (b), and (c), the first, second and third plots represent the SLA as a function of longitude, the LWPS (energy units in cm^2) as a function of longitude and wavelengths, and the bathymetry as a function of longitude, respectively. For the LWPS, the parabolic black line delimits the cone of influence (Torrence and Compo, 1998). The black lines represent the 95% confidence level of the wavelet coefficient (χ^2 statistical test).

December). The same double-wavelength WT spectrum is occasionally observed in other periods, such as at the beginning of 1994, but 1998 is the only year in which it lasted for several months. To illustrate, the WT spectrum for the same latitude in April 1995 is represented in Figure 3c. For the latter, we observe only a continuum of wavelengths from

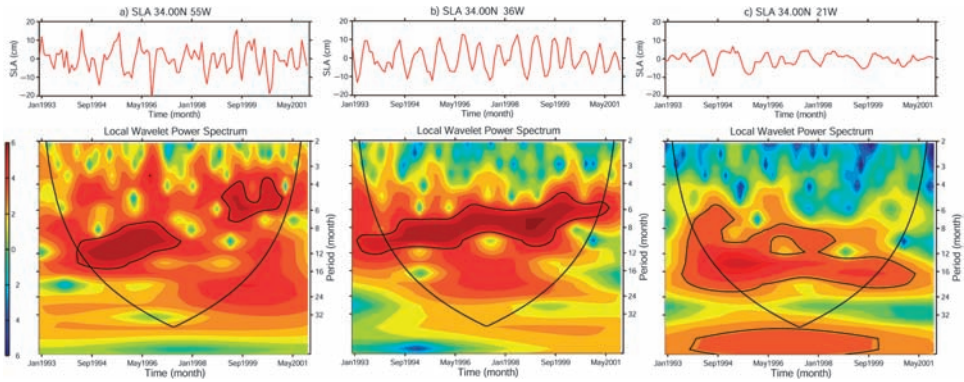

Figure 4. Temporal LWPS (energy units in cm^2) at 34N: (a) 55W, (b) 36W, and (c) 21W from filtered SLA. For (a), (b), (c) the first and second diagrams represent the same two first plots than for Figure 3 (a, b, c) except that longitude is replaced by time, and wavelengths by periods.

500 km to 1000 km, rather than two distinct peaks. The position of wavelet coefficient maxima is generally correlated with the mid-Atlantic ridge. For example, at 34N, signals with high amplitude are detected above the ridge and persist west of the ridge. Establishing a trend at other latitudes is less obvious, but in general it seems that, north of 28N, energy is higher above and west of the ridge than to the east of it. According to Polito and Cornillon (1997), a coupling between baroclinic and barotropic modes may be responsible for the wave amplification above the ridge. As shown originally by Barnier (1988), on approaching the ridge the baroclinic wave energy is transmitted to the barotropic mode; the converse happens on the western flank of the ridge. The new baroclinic waves then generated over the ridge and associated to local wind stress fluctuations may explain the amplitudes observed. An analysis of wind stress fluctuations above the ridge may therefore help to explain the intensification of the signal, but is beyond the limits and scope of the present study.

To characterize the Rossby wave periods, we use a temporal wavelet analysis on the data filtered and reconstructed from the spatial wavelet coefficients for wavelengths between 500 km and 1000 km. This analysis shows the temporal period of the corresponding signal at a given location in longitude and latitude on the complete data series. Results (Fig. 4) are presented for three chosen points along the 34N parallel: east, above and west of the ridge. A general decrease of the period can be observed from the east to the west side of the ridge. At 21W, east of the ridge, periods between $\sim$ 12 and $\sim$ 16 months present a significant energy (Fig. 4c). Above the ridge, Rossby wave periods decrease with time from $\sim$ 10 to $\sim$ 6 months (Fig. 4b). In the western part of the basin, no coherent structure can be observed in the wavelet coefficients. Only sparse patches exist for periods between $\sim$ 6 and $\sim$ 16 months (Fig. 4a).

The temporal analysis extended to other latitudes between 10N and 40N shows a strong meridional variability (Fig. 5). However, a trend toward a northward increase of the period

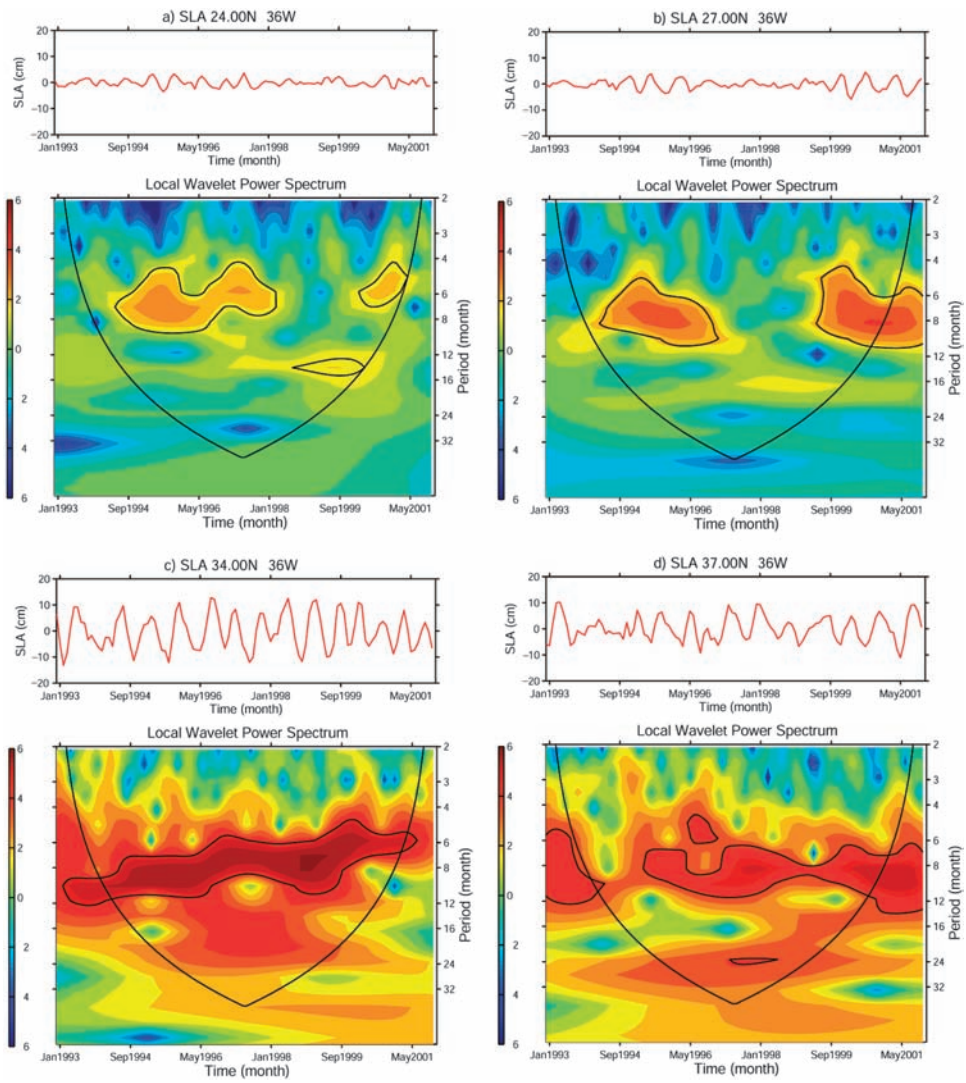

Figure 5. Temporal LWPS (energy units in cm^2) at (a) 24N , (b) 27N, (c) 34N, and (d) 37N and 36W from filtered SLA. For (a), (b), (c), (d), the first and second diagrams represent the same plots as in Figure 4.

is observed on the local wavelet power spectrum, with periods between $\sim$ 4 and 12 months south of 30N (Figs. 5a, b) and between $\sim$ 6 and 24 months north of 30N (Figs. 5c, d). These results are in agreement with the observations from Polito and Liu (2003). Indeed, between the wavelengths $\sim$ 500 and $\sim$ 1000 km, they detected the existence of periods around 3 months south of 20N, around 6 months between 20N and 30N, and around 12 months north of 30N.

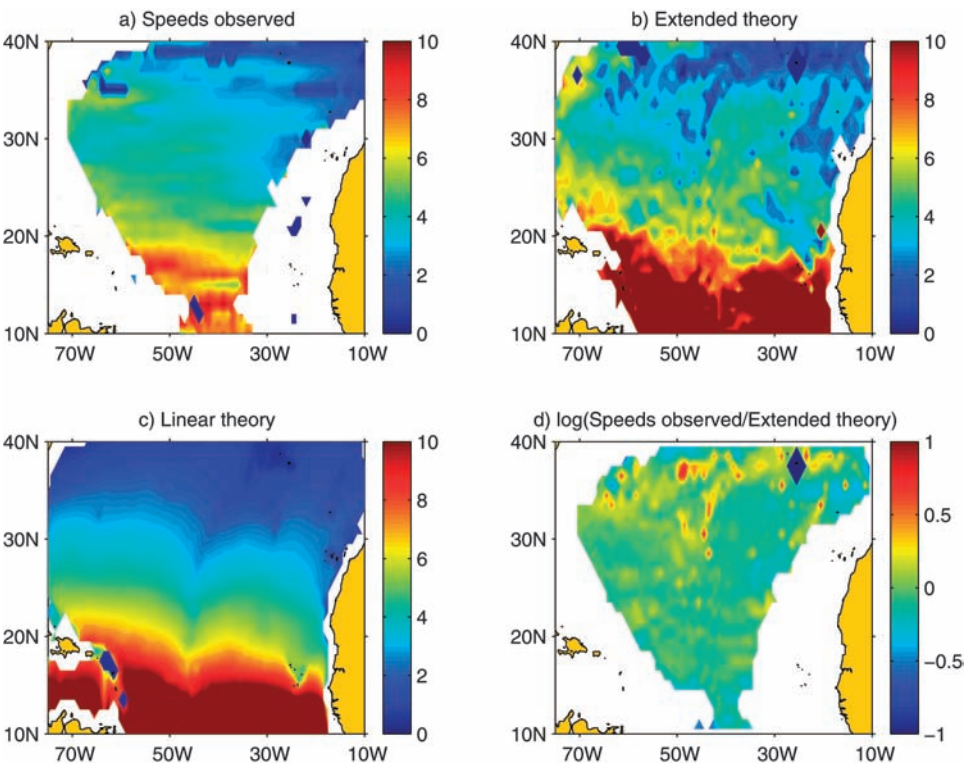

Figure 6. Propagation speeds (cm s^{-1}, positive westward) corresponding (a) to the filtered SLA data (speeds were computed with the 2-D Radon transform (see Challenor *et al.*, 2001)), (b) to the extended theory (Killworth and Blundell, 2003), (c) to the linear theory. (d) Logarithm of the ratio between speeds deduced from the observations and the extended theory. In (a) and (d), data close to the coasts are omitted due to strong zonal chlorophyll gradients which introduce marked edge effects in the wavelet analysis.

iii. Phase velocities. Propagation velocities (or phase speeds) associated with Rossby waves (500 – 1000 km) are now calculated from the filtered time/longitude diagrams with a 2-D Radon transform method (for details see Challenor *et al.*, 2001).

For the SLA, the values of the velocities increase equatorwards, from 1-2 cm s^{-1} to more than 20 cm s^{-1} (Fig. 6a). Such a dependence on latitude is expected from both the linear theory for the first baroclinic mode of Rossby waves and its more recent extensions (Fig. 6b, c). We also observe a westward increase of the speeds, which is well described by the extended theory from Killworth and Blundell (2003a, b). This theory gives a better representation of these increases because it considers the bathymetry (and particularly the mid-Atlantic ridge) and the mean currents. For example, at 34N, velocities vary between 1 to 6 cm s^{-1} from east to west of the basin in the observations.

The observed phase speeds are in broad agreement with the velocities that the extended theory from Killworth and Blundell (2003a, b) predicts for the first baroclinic mode,

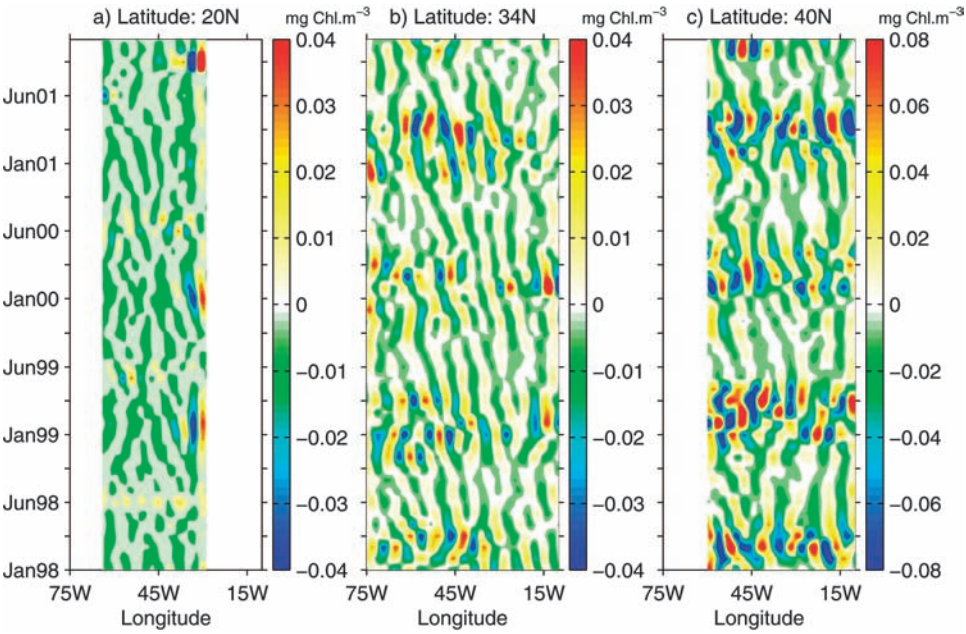

Figure 7. Time/longitude plots for chlorophyll-*a* concentrations (mg Chl m^{-3}) at (a) 20N, (b) 34N and (c) 40N. Data have been spatially filtered. Signals are reconstructed for wavelengths between 500 and 1000 km using a wavelet analysis.

therefore it is safe to assume that in the majority of locations they represent the first baroclinic mode of Rossby waves. However, the ratio between observed and theoretical speeds (Fig. 6d) still shows some strong differences in a few localized areas; for example, north of 33N in the western part of the basin where there are areas of significantly faster propagation than predicted, and in a few spots in the southern and eastern part of the study region, where observed waves are slower than predicted. The presence of some residual discrepancies between theoretical and observed speeds is in line with the results of a number of studies (reviewed in Fu and Chelton, 2001).

iv. Spatial and temporal properties from chlorophyll-a concentrations. We now move to the observation of planetary waves in the chlorophyll data set. As reported in previous studies (Cipollini *et al.*, 2001; Uz *et al.*, 2001), westward-propagating features can be detected on time/longitude diagrams of ocean color data; here we show three examples in Figure 7, computed with the same method as for the SLA in Figure 1. The observed features are very similar to the Rossby waves detected in SLA, with wavelengths between 500 km and 1000 km. However, the amplitudes are perturbed by the strong residual seasonal cycle on chlorophyll-*a* concentrations data. At 34N above the ridge, the chlorophyll-*a* concentrations amplitudes (Fig. 7) linked to Rossby waves do not seem amplified as for SLA amplitudes.

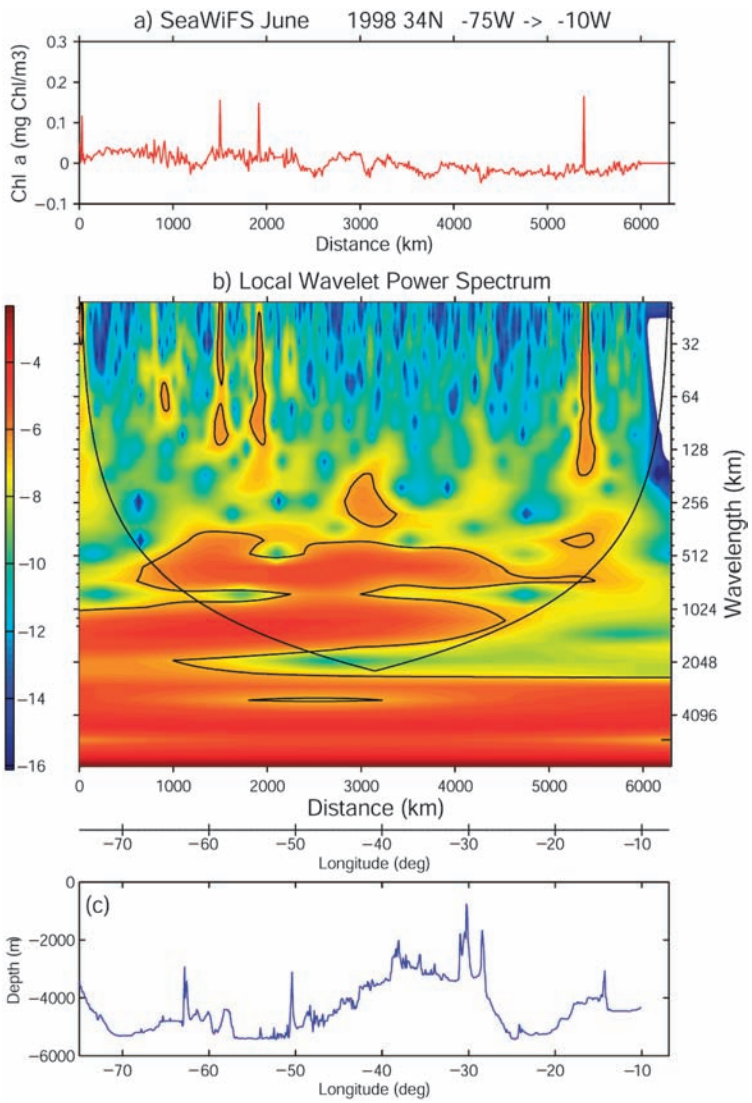

Figure 8. Spatial LWPS (energy units in (mgChl m^{-3})^2) at 34N in June 1998 of chlorophyll-*a* concentrations. The first, second and third diagrams represent the same plots as in Figure 3 (a, b, c) except that SLA is replaced by chlorophyll-*a* concentrations.

To compare the particular signals observed in the SLA in 1998 with the chlorophyll-*a* concentrations, we again use the spatial wavelet analysis. The signatures for both wavelengths 500 km and 1000 km (Fig. 8) are observed but not for the entire year. Both wavelengths are relatively well detected from January to June and are absent from July to November.

At 34N, from January to June, this latitude is occupied by a strong chlorophyll front between the oligotrophic subtropical gyre and the highly productive mid-latitudes. The front slopes north-eastward, on average between ~35N on the American shelf to ~45N off Europe, but presents some meridional variability. The seasonal variation in the position of the front, in particular, could play an important role in the signature of Rossby waves in chlorophyll-*a* concentrations. As we see through the wavelet analysis at 28N, 34N and 40N, the detection of typical wavelengths of Rossby waves is strongly correlated with the position of the front (Fig. 9). Indeed, larger energy at wavelengths compatible with planetary waves is detected when the front (strong meridional gradients of chlorophyll-*a*) is centered on these three latitudes. In February, the southern limit of the chlorophyll-*a* front extends to 28N (Fig. 9j) and Rossby wave signatures can be detected (Figs. 9a, d, g for each latitude 40N, 34N and 28N, respectively). In April, Rossby wave signatures are observed at 34N (Fig. 9e) and 40N (Fig. 9b) due to a southern front extension slightly south of 34N (Fig. 9k). In July, the front presents a weak southern extension and the strongest values of the chlorophyll-*a* meridional gradients appear only north of 34N (Fig. 9l). In this case, Rossby wave signatures are mostly observed at 40N (Fig. 9c, f, i). These observations suggest that horizontal advection of meridional gradients should play an important role in the formation of an ocean color signal, but do not allow ruling out other mechanisms, which will be examined in the coupled SLA/chlorophyll study in Section 3.

v. 1998: A particular year? In this subsection we examine the presence of two distinct wavelengths in 1998 at 34N in both SLA and chlorophyll-*a* data sets. The first question is to confirm the nature of these two distinct components as planetary waves; to this purpose, the range of wave numbers (~500 km to ~1000 km) and frequencies (~4 to 24 months) observed in the analysis is compared with the dispersion relation of the linear theory (calculated from the 2001 World Ocean Atlas of temperature and salinity data; Conkright *et al.*, 2002) (Fig. 10). A broad agreement is obtained between the data and the first baroclinic mode. Part of the residual discrepancy between observations and theory can be explained with the presence of a mean zonal current and of a noflat bottom topography, two of the improvements added by the extended theory (Killworth *et al.*, 1997; Killworth and Blundell, 2003a, b); observed speeds will however be faster than theory in a few localized spots at 34N. A cross-spectral analysis based on time/space 2D Fourier transform was carried out between the weekly wind stress and wind stress curl (from the NCEP data set, Kalnay *et al.*, 1996) and the SLA. Apart from sporadic correlation peaks at smaller temporal scales (~ 5 months periods) above the ridge and west of the basin (not shown), it is hard to find any significant link between the wind conditions in 1998 and the signature of Rossby waves on SLA. The influence of STORM (SubTropical Oceanic Rings of Magnitude) eddies, which have physical properties close to Rossby waves (Pingree and Sinha, 1998), was also investigated. According to the observations of Mouriño *et al.* (2003), eddies can be seen east and above the ridge, but only two STORM eddies were observed in 1998 east of 24W. Then, it looks unlikely that they can explain the particular

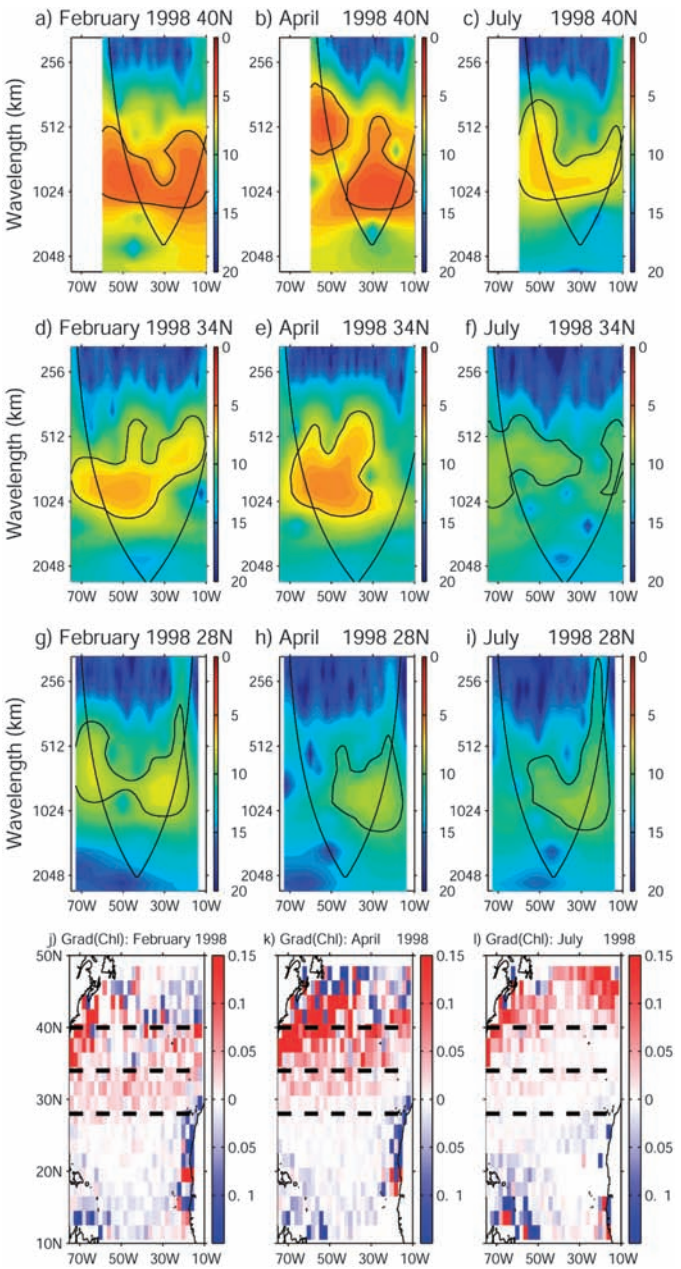

Figure 9. Spatial LWPS (energy units in (mgChl m^{-3})^2) at 40N (a, b, c), 34N (d, e, f) and 28N (g, h, i) in February (a, d, g), April (b ,e ,h) and July 1998 (c, f, i). The chlorophyll-*a* concentrations are filtered with a wavelet analysis for wavelengths between 500 km and 1000 km. Meridional gradients (1/degree) of the $\log_{10}$(chl) from the SeaWiFS data set are represented for February (j), April (k), and July (l). The three dotted black lines indicate the three latitudes described in the LWPS.

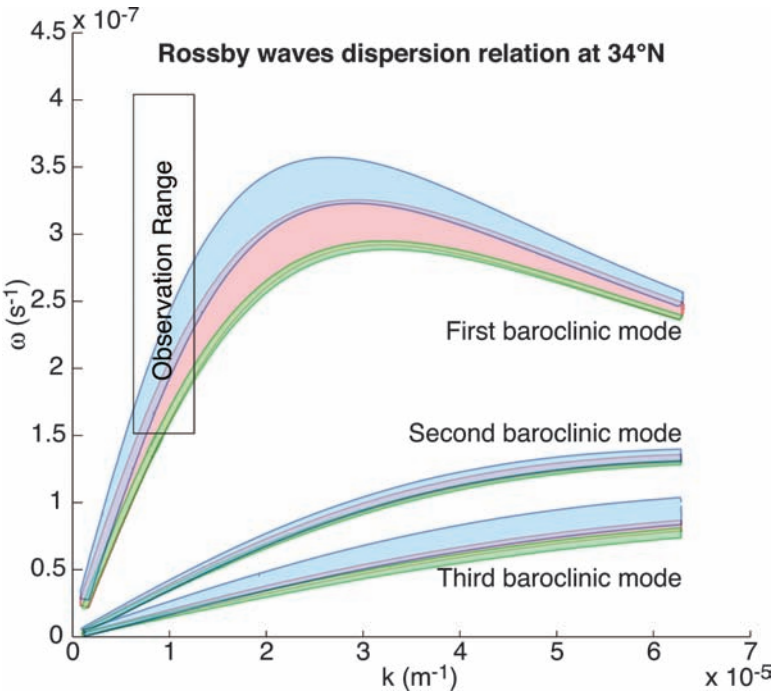

Figure 10. Relation of the linear theory of Rossby waves for the first three baroclinic modes of Rossby waves (calculated from the World Ocean Atlas 2001 of temperature and salinity data; Conkright *et al.*, 2002). The green, red and blue envelopes represent the eastern part of the basin (25W-10W), the domain above the ridge (50W-25W), and the western part of the basin (74W-50W), respectively. The rectangle delimits the area which corresponds to the observations (with wavelengths from 500 km to 1000 km for periods between 6 and 16 months).

signals we observed in 1998 (maxima of wavelet coefficients are detected from 30W to the west of the ridge). The question of the origin of these two distinct wave components at 34N therefore remains open, and *in situ* data as well as 3D modeling will have to be used to explore the vertical stratification associated to the different wavelengths in order to understand the observed surface signals.

3. Signature of Rossby waves in chlorophyll-*a* concentrations and SLA: A coupled process

a. Joint SLA/chlorophyll concentration remotely sensed data analysis

The signature of Rossby waves on ocean color can, in principle, be due to a number of different mechanisms. In this section we address the question of which mechanism dominates in the North Atlantic, following and extending the "modeling versus cross-spectra" approach recently suggested by Killworth *et al.* (2004). Their global study

introduces process models that provide valuable information to investigate the different coupled processes involved in the Rossby waves signature at different locations in the ocean. In particular, the amplitude and phase relationship between surface chlorophyll-*a* concentrations and SLA can be predicted theoretically for each mechanism and can be compared with the cross-spectral observations in an attempt to assess the relative importance of that mechanism.

The three processes described in the introduction can be classified in horizontal (the horizontal advection of meridional chlorophyll gradients) and vertical (the uplifting of the chlorophyll subsurface maximum and the upwelling of nutrients). In the case of a spatial analysis, it can be demonstrated theoretically that the predicted spatial phase relationship associated with vertical processes is between $\pi/2$ and π (Killworth *et al.*, 2004). For the horizontal mechanism, the theoretical phase relationship depends on the sign of the meridional gradient of chlorophyll and the hemisphere studied. In the North Atlantic Ocean, two situations can be observed: (1) roughly north of 28N, a positive meridional gradient of chlorophyll ($\partial[Chl]/\partial y > 0$) which gives a spatial phase relationship between $\pi/2$ and π, and (2) south of 28N, a negative gradient of chlorophyll ($\partial[Chl]/\partial y < 0$) which gives a phase relationship between $-\pi/2$ and 0.

Here we analyse the relationship between the chlorophyll and SLA signal by means of a cross-wavelet approach, which allows us to characterize the temporal variability of the phenomena. Wavelet coherency and phase (phase (chlorophyll-*a*) – phase (SLA)) are computed for each latitude from 10N to 40N and for each month from January 1998 to December 2001 which is the coincident period for the two remote data sets (prior to the cross-wavelet analysis, the data were rebinned onto a 1° x 1° grid to reduce the noise level). The cross-wavelet analysis (see Appendix) is applied to the wavelet-filtered data. We then extract, from each Local Wavelet Power Spectrum, the phase for components between 467 km and 1110 km wavelength (in the cone of influence, to exclude the edge effects), having a coherency above 0.75. Tests have been performed on this coherency threshold and for threshold values above 0.75, the phases do not change significantly. The largest coherency is observed north of 30N, where it reaches values above 0.95 (not shown). This strong coherency appears to be correlated with the strongest amplitudes of Rossby waves in SLA and in chlorophyll-*a* concentrations. In fact, south of 28N, the amplitudes are very small which could explain why the wavelet analysis cannot detect significant periodic signals (not shown). Figure 11 presents the maps of these phase relationships (phases for coherency lower than 0.75 are not plotted) for the month of April, from 1998 to 2001. It shows a strong interannual variability but we can observe some large scale spatial features, and a clear difference between the northern and southern parts of the study area.

In the area of strong positive meridional gradient (starting a bit to the north of 28N, i.e. roughly at 30N), phases are mainly between $\pi/2$ and π, most clearly in April 1998 and 2001 (Figs. 11a, d). However in this area where the meridional gradient of chlorophyll-*a* is positive, such a range of phase values can arise from both vertical and horizontal processes,

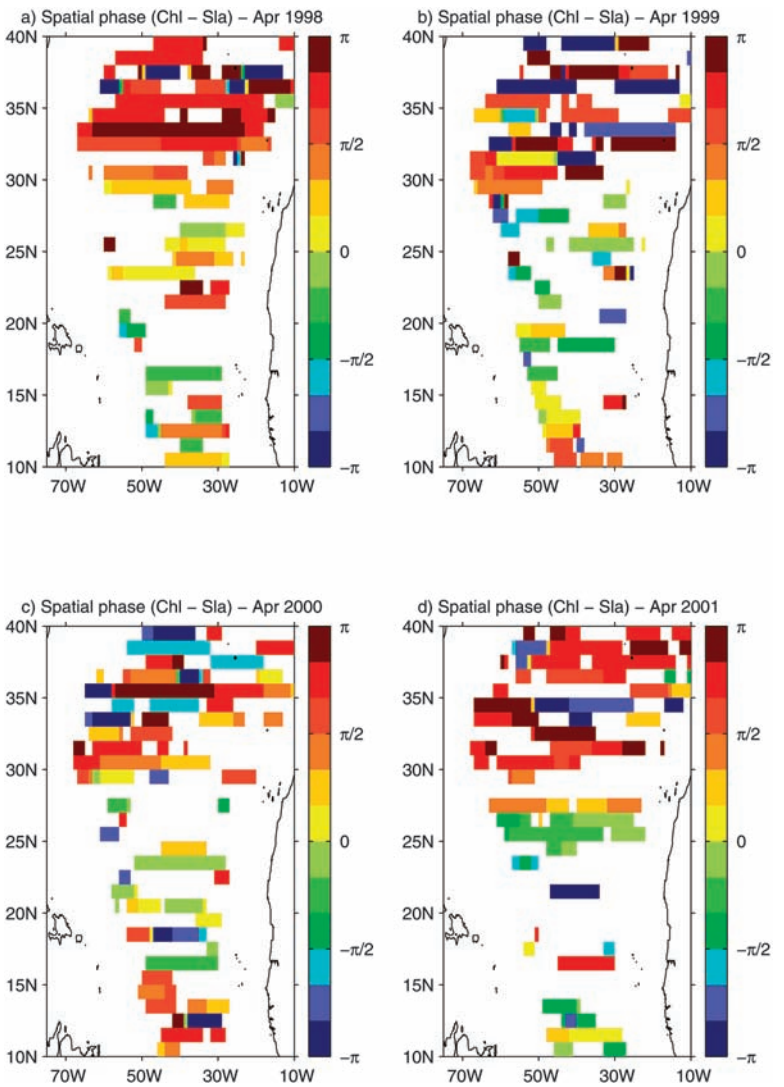

Figure 11. Phase relationships between SLA and chlorophyll-*a* concentrations (phase(chlorophyll-*a*) – phase(SLA)). They were computed using the cross-wavelet analysis. Phases for the data having a maximum coherency >0.75 are extracted from each LWPS in the cone of influence for wavelengths between 467 km and 1110 km. In case more than one data set has the same maximum coherency in the spectral domain, the point, in the physical space, is excluded to retain only unambiguous phases. To describe the temporal variability, the month of April from 1998 to 2001 (a to d) is displayed.

and the determination of a dominant mechanism remains ambiguous at this stage. For the particular case of 1998 at 34N, a strong coherency is observed separately for the two distinct wavelengths (~500 km and ~1000 km) from April to June and the phases associated to these two maxima are similar (around π - not shown).

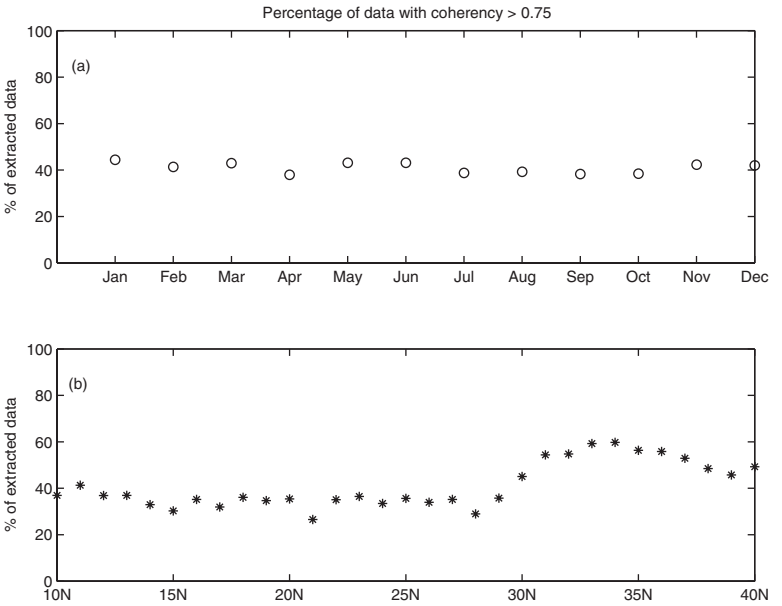

Figure 12. Ratio of extracted data compared to the number of data used for the cross-wavelet analysis (expressed in %) (a) monthly averaged, and (b) zonally averaged for the whole period (1998-2001).

In the weak gradient zonal band around 28N and south of that band, the observations are less coherent and very noisy. Horizontal advection could explain the Rossby wave signatures in surface chlorophyll-*a* concentrations in all those locations where the observed phases are between -π/2 and 0. On the contrary, vertical processes would still generate a phase between π/2 and π, which is only observed in a very small number of grid points. Therefore in this region the phase observations point unequivocally to horizontal advection as the predominant process, confirming the findings of Killworth *et al.* (2004).

The analysis detailed above for the month of April has been repeated for other months leading to similar results. The percentage of data having a coherency above 0.75 is approximately the same (between 34 and 49% with a mean value of 41%) for each month and each year studied. The analysis of the percentage of extracted data as a function of latitude confirms that north of 28N there is better chlorophyll-*a* concentrations/SLA coherency, with values above 50% (Fig. 12). The maximum of this percentage is reached for the 34N latitude (59.7%).

To summarize the results of the wavelet cross spectral analysis, despite some degree of temporal variability (and higher noise south of 28N) the phase relationship appears to be in good agreement with the average temporal phase map found by Killworth *et al*. (2004) over the entire time series (their Fig. 6h) when one considers that due to the propagation being westward, the spatial phases computed here will have opposite sign.

b. Coupled physical and biological process modeling

The attribution of the ocean color signal to different mechanisms suggested in the previous subsections has been mainly based on qualitative considerations. In this subsection, instead, we take a more quantitative look at the amplitude ratios and phase differences between chlorophyll concentrations and SLA, trying to identify the shares of the processes that can explain the chlorophyll signature of Rossby waves and resolve any ambiguity if possible. First we will illustrate this approach at three test latitudes (representative of different background conditions), then we will extend it to the whole region. The phase and amplitude relationships are computed for the three different mechanisms and are compared to the observed relationship, in agreement with Killworth *et al.*'s (2004) approach, which is recalled below.

i. Model used (Killworth et al., 2004). Killworth *et al.* (2004) describe the evolution of a tracer (C) advected by a purely westward propagating Rossby wave. In such wave, the mean north-south flow ($\bar{v}$) is weak compared with the mean east-west flow, so $\bar{v} = u' = 0$. The following linearization of the advection/diffusion equation is taken:

$$C'_t + \bar{u}C'_x + v'\overline{C_y} + w'\overline{C_z} = M \tag{1}$$

where the axes are x east, y north and z upward (with respective velocities u, v, w). The suffixes denote perturbation around the mean value (noted ') or differentiations over time t or space. M represents all the nonconservative processes for the tracer. w' is estimated from the vortex stretching equation ($\beta v' = f w'_2$) where f *is* the Coriolis parameter and $\beta = df/dy$ the northward gradient of the Coriolis parameter. Eq. (1) is integrated over an ocean surface layer of depth h.

Based on this integrated advection/diffusion equation, a complex expression of the ratio between the amplitude of the tracer signal (C_A) and the sea-surface height (η_A), sufficient to express the various possible combinations of mechanisms, is obtained:

$$\frac{C_A}{\eta_A} = \left|\frac{C_A}{\eta_A}\right| e^{i\varphi} = \frac{g}{f}\frac{(\bar{C}_{0y} - \beta\Delta C/f)}{(c - \bar{u}_0 + ic/\omega\tau)} \tag{2}$$

where φ is the phase difference, g is the acceleration due to gravity, c the phase speed of the wave, ω the wave frequency. $\bar{C}_{0y}$ is the horizontal meridional gradient of tracer. The assumed limiting nutrients are the nitrates which is a good approximation over the North Atlantic Ocean. $\Delta C \equiv \overline{C}(z = 0) - \overline{C}(z = -h)$ with $h = 50$ m for nutrients (chosen value for the mixed layer depth using the more recent nitrate climatology of Louanchi and Najjar (2001) and $h = 10$ m for chlorophyll (for the reasons outlined by Killworth *et al.*, 2004). τ is the relaxation time, i. e. the characteristic decay time of the tracer anomaly, here taken to be 20 days with $M_0 = -C'_0/\tau$. $\bar{u}_0$ is the mean zonal current. All the chosen values for the different parameters are taken from Killworth *et al.* (2004).

Eq. (2) allows the modeling of the three different mechanisms. The horizontal advection case is computed by taking C as chlorophyll concentrations and removing the effect of the

vertical advection ($\Delta C = 0$). The vertical advection processes are simulated removing the tracers gradients ($\bar{C}_{0y} = 0$), then taking C to represent either chlorophyll concentrations to solve the vertical advection of chlorophyll, or nutrient concentrations (then converted to chlorophyll assuming a constant Chl:N ratio $\Delta C = 1.59\ \Delta N$) for the upwelling case. Using these different formulations, amplitude ratios and phase relationships from each process can be analyzed.

ii. Remotely sensed observations (Killworth et al., 2004). Although the wavelet analysis described in Section 3a describes amplitude and phase between SLA and ocean color as a function of space and time, the theoretical model (6) is independent of time; in order to compare observations and model we would need to take some kind of time average of wavelet cross-spectra in time. We will therefore use the amplitude ratios and phase relationships computed by Killworth *et al.* (2004) with a cross-spectral Fourier analysis between SLA and surface chlorophyll concentrations, as these already represent averages over the entire time series. The cross-spectral complex coefficients allow a precise quantification of the average (over the time series) amplitude and phase relationship of the two signals at those frequencies and wave numbers at which they are most correlated. Then these relationships can be directly compared to those from the theoretical simulations.

iii. Combining model and observations: a dominant mechanism in the North Atlantic? The detailed comparison between the model and the observations has been performed at three given model grid latitudes: 33.5N, 23.5N and 19.5N. These latitudes correspond to three areas with different chlorophyll concentration distributions. 33.5N is close to the 34N latitude studied before with the remotely sensed data, and corresponds to the front position normally associated with large positive meridional gradients of chlorophyll concentrations. The second latitude, 23.5N was selected to describe the different processes in the middle of the subtropical gyre characterized by low surface chlorophyll concentrations and weak horizontal surface chlorophyll gradients. The third latitude, 19.5N, is also located in the subtropical gyre (oligotrophic zone) with negative meridional gradients of chlorophyll concentrations but exhibits stronger vertical chlorophyll gradients between 0 and 10-meter depth (from Conkright *et al*., 1998). Using these three latitudes we can analyze the mechanisms involved following different chlorophyll backgrounds: strong positive meridional chlorophyll gradients (33.5N), weak horizontal and vertical gradients (23.5N) and strong vertical chlorophyll gradients with weak meridional chlorophyll gradients (19.5N).

First, we compared the observed phase relationships to the theoretical model as it was previously performed using the wavelet analysis. The observed phases for the latitude 19.5N extend between 0 and $\pi/2$ (Fig. 13d) in good agreement with the modeled phases from the horizontal advection process. This result suggests that horizontal advection of meridional chlorophyll gradients by Rossby waves may be responsible for a large part of the observed features in the chlorophyll data, notwithstanding the strong vertical gradient.

At 23.5N, despite slightly different conditions, the observed phase relationships (between 0 and $\pi/2$) are very similar to those at 19.5N, also in favor of the horizontal

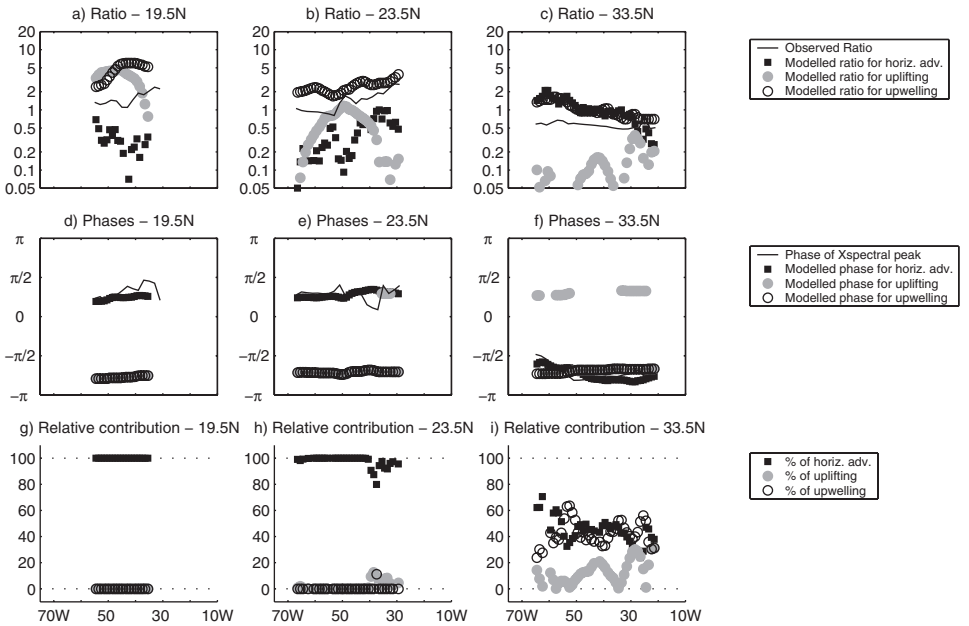

Figure 13. Amplitudes ratio (tracers on SLA) from the remotely sensed data (black line), modeled for the horizontal advection process (square) and modeled for the vertical processes (full grey circle for the chlorophyll uplifting and empty circle for the nitrate upwelling) for the latitudes 19.5N (a), 23.5N (b) and 33.5N (c). With the same symbols, the observed and modeled phase relationships are represented on the diagrams (d) for the latitude 19.5N, (e) for 23.5N and (f) for 33.5N. The three bottom diagrams represent the relative contribution (in %) of the three assumed processes for the latitudes 19.5N (g), 23.5N (h) and 33.5N (i).

advection process (Fig. 13e). We notice a jump in phase for four points located in the eastern part of the basin for the modeled phase relationship of the chlorophyll uplifting (the associated values lie between 0 and $\pi/2$ compared to the $[-\pi,-\pi/2]$ range found for the other longitudes). After analyses of the chlorophyll climatology used in this theoretical model (Conkright *et al.*, 1998), it appears that these artefacts are linked to an inaccurate climatology in this region (due to few data and interpolation method) because these variations correspond to sign changes of the vertical gradient (surface chlorophyll concentrations are greater than subsurface concentrations). We then exclude these points (the same applies to a few locations at 33.5N) from our study.

At 33.5N, the phase range deduced from the theory is the same for the horizontal and vertical mechanisms as mentioned in Section 3a. All the modeled phases are in the same quadrant as the remotely sensed data, between $-\pi$ and $-\pi/2$ (Fig. 13f). Then, using the phase information without additional assumption, the three mechanisms can contribute.

Our strategy to investigate the relative contributions of the three different coupled processes is precisely to add a statistical assumption that allows a quantitative decomposi-

tion of the contributions by the different processes, by combining together modeled and observed amplitude ratios and phase relationships.

The assumption we use is to consider the observed amplitude ratios and phases as a linear combination of the three modeled processes. So, the following equation can be built:

$$\left|\frac{C_A}{\eta_A}\right|_{obs} e^{i\varphi_{obs}} = z_\alpha \left|\frac{C_A}{\eta_A}\right|_{hadv} e^{i(\varphi_{hadv})} + z_\beta \left|\frac{C_A}{\eta_A}\right|_{upl} e^{i(\varphi_{upl})} + z_\gamma \left|\frac{C_A}{\eta_A}\right|_{upw} e^{i(\varphi_{upw})} \tag{3}$$

where z_α, z_β and z_γ are three unknown parameters associated with the different modeled complex amplitudes: horizontal advection, chlorophyll uplifting and nitrates upwelling processes, respectively. These parameters are complex (for example $z_\alpha = \alpha \exp(i\,\varphi_\alpha)$) in order to encompass both an amplitude and a phase error in the model.

System (3) has six unknown parameters for two equations (real and imaginary parts) so it has an infinite number of solutions. Among the different possible solutions, we select the one that gives the smallest value for the following cost function:

$$\Psi = \sqrt{|z_\alpha - 1|^2 + |z_\beta - 1|^2 + |z_\gamma - 1|^2} \tag{4}$$

Cost function Ψ describes the distance, in parameters' space, between the three complex parameters and number one, based on the idea that if the process modeling is correct then all the three coefficients would be equal to unity. In other words, z_α, z_β or z_γ equal one represents a total contribution by the corresponding process, exactly as modeled (that is, with exactly the modeled amplitude and phase), to reproduce the observations. Solving (3) by minimizing Ψ allows extracting a set of parameters to reproduce the observed amplitude ratios and phase relationships. The relative contributions (*P*) are then computed using the following equation:

$$P_j = 100 \times \frac{z_j \left|C_A/\eta_A\right|_j}{z_\alpha \left|C_A/\eta_A\right|_\alpha + z_\beta \left|C_A/\eta_A\right|_\beta + z_\gamma \left|C_A/\eta_A\right|_\gamma} \tag{5}$$

where $j = \alpha, \beta, \gamma$.

We then applied this method to the three selected latitudes. It appears that at 19.5N and 23.5N, the horizontal advection is clearly the main process (Figs. 13g, h). This result is in agreement with our previous conclusions from phases relationships (observed and modeled). For the latitude 33.5N, this new approach highlights not only a clear contribution by the horizontal advection as suggested by the good correlation between the signal detected and the chlorophyll front position (see Section 2c.*iv*), but also a contribution by the nitrate upwelling process (Fig. 13i). In short, the observed chlorophyll signature of Rossby waves at 33.5N seems to be due to a combination of a vertical and a horizontal process. The upwelling of nitrates and the horizontal advection of the chlorophyll gradients might explain, each one, around 50% of the observed amplitude ratio.

For a global view of the influences of Rossby waves in this part of the North Atlantic Ocean, we applied the method for all latitudes from 10N to 40N. Figure 14 shows the

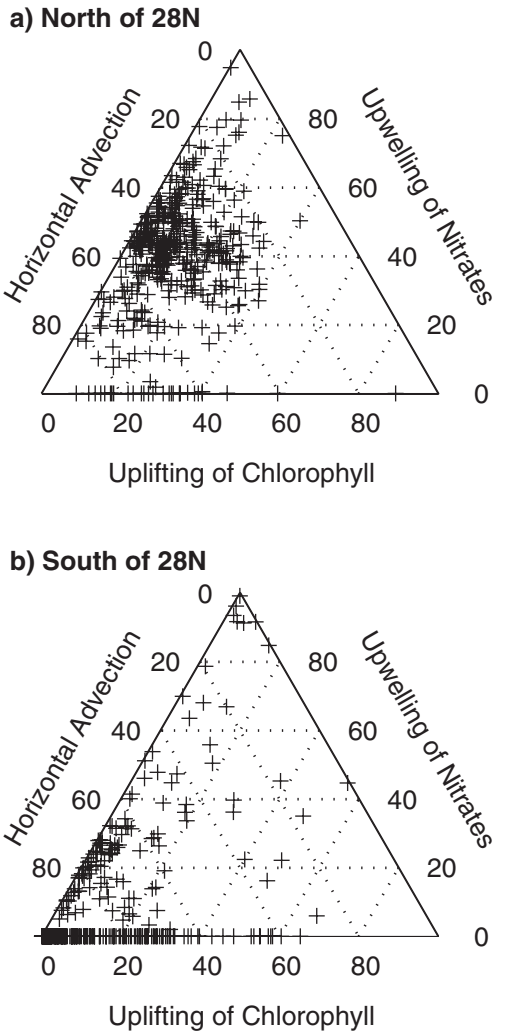

Figure 14. Relative contribution (in %) of the three assumed processes which can explain the chlorophyll signature of Rossby waves: horizontal advection of meridional chlorophyll gradients, upwelling of nitrates in the euphotic zone and uplifting of the deep chlorophyll maximum. The crosses represent all the model grid points north of 28N (a) and south of 28N (b) between 9.5N and 40.5N.

relative contribution, computed from Eq. 5, of the three assumed processes for each model grid points north of 28N (Fig. 14a) and south of 28N (Fig. 14b) between 9.5N and 40.5N. The values obtained are then represented on a ternary diagram. North of 28N, the diagram shows values centered around 50% of horizontal advection of chlorophyll gradients and upwelling of nitrates. The relative contribution of uplifting of chlorophyll is lower than

35%. South of 28N, there is a main contribution of the horizontal process with most of values higher than ~ 70%. The vertical processes can reach a relative contribution of 35% in the case of the uplifting of chlorophyll and 25% for the upwelling of nitrates. At these latitudes, the horizontal process is clearly dominant.

In summary, the results highlight two main regions already previously found with the phases relationships deduced from the remotely sensed data (Section 3a). South of 28N, the horizontal advection of chlorophyll gradients is the dominant process with a contribution higher than ~ 70% of the observed amplitude ratios (Fig. 14b). North of 28N, the upwelling of nitrates and horizontal advection processes contribute approximately by the same amount to explain the observed amplitude ratios (Fig. 14a).

4. Conclusions

The detailed analysis of remotely sensed data with spatial and temporal wavelet analysis allows us to characterize Rossby wave variability in the North Atlantic Ocean. The main features are in agreement with previous work and the peculiarity of the wavelet method yields additional details about these waves and their characteristics. Signals with wavelengths between ~ 500 km and ~ 1000 km and with ~ 4- to ~ 24-month periods were detected and identified as the first baroclinic mode of Rossby waves, as observed by Polito and Liu (2003), and Osychny and Cornillon (2004). The propagation speeds estimated with the Radon transform have been compared to the extended theory from Killworth and Blundell (2003a, b) and confirm that we observed the first baroclinic mode of Rossby waves. However there are still areas in the basin where significantly faster waves are observed.

The spatial and temporal information given by the wavelet analysis have also allowed to highlight a particular situation in 1998 at 34N, with the simultaneous existence of two wave components corresponding to wavelengths 500 km *and* 1000 km. Analysis of the wind field was not conclusive on the cause of the existence of these two distinct signals for this particular year and latitude, therefore further studies are needed.

The main finding of the paper is a quantification of the relative importance of various mechanisms explaining the signature of Rossby waves on ocean color. Although already explored by several authors, the problem is difficult to solve in a deterministic way. With the current tools and data from several regions in the oceans, an answer can only be given by taking additional statistical assumptions. The study of the spatial phase relationship between the surface chlorophyll-*a* concentrations and the SLA led to some interesting considerations in the North Atlantic Ocean. North of 28N, the spatial phase relationship does not allow decoding the dominant process unambiguously. South of 28N, the weak coherency between chlorophyll-*a* concentrations and SLA decreases significantly the number of data that can be used to analyze the phase. Nevertheless, it is found that most of the phases range between $-\pi/2$ and $\pi/2$. Thus, phases observed at these latitudes are mostly in agreement with the horizontal process but caution is of use here due to the low number of points and the noisiness of the results. With this cross-wavelet analysis, the temporal

variation of chlorophyll/SLA phase relationships has been addressed. Over these 4 years of data, monthly phase relationships do not change significantly. The use of the theoretical model from Killworth *et al.* (2004) compared to the observations, confirms results obtained with the cross-wavelet analysis. The two latitudes, 19.5N and 23.5N analyzed south of 28N presents a clear agreement between the observations and the horizontal advection mechanism simulated.

The exploration of the relative contribution of the three different processes using the theoretical model and the remotely sensed data, and adopting a statistical cost function, leads to the conclusion that north of 28N, the chlorophyll signature of Rossby waves may not be due to a horizontal process alone. In fact, our analysis shows that upwelling of nitrates in the euphotic zone can explain about half of the observed amplitudes. This observation is coherent with the vertical nitrate gradients from the climatology. The other part is due to horizontal advection, in agreement with the good correlation found between the signal observed and the chlorophyll front position. Some caveats have to be made on these results knowing the different strong assumptions made in the Killworth *et al.*'s (2004) model (for example, the constant Chl:N ratio, and a constant decay time for the chlorophyll anomalies, which are both first-cut approximations). However our findings suggest that Rossby waves may have an influence on the biological production in this part (north of 28°) of the Atlantic Ocean. In future work, simulated chlorophyll fields from a coupled physical/biological model over the North Atlantic Ocean will be used to understand the contributions of the different processes in the surface chlorophyll concentration signature and to quantify the influence of Rossby waves on the primary production.

Acknowledgments. Financial support for this work was provided by the GMMC (Groupe Mission MERCATOR/CORIOLIS) to LEGOS. The CNES and IFREMER are thanked for the fellowship attributed to G. Charria. We would like to thank the Université Paul Sabatier for the ATUPS financial support during G. Charria's stay at NOCS. Ocean color data were produced by the SeaWiFS project at GSFC and obtained from the DAAC. We thank J. Sudre (LEGOS) for extracting the SeaWiFS data. Wavelet software was provided by C. Torrence and G. Compo, and is available at http://paos.colorado.edu/research/wavelets/. The NCEP data set was kindly provided by Simon Josey (NOCS). We are grateful to J. Blundell, D. Cromwell and P. Killworth from NOCS, X. Carton from LPO, and J. Sudre for their remarks and suggestions as well as the two anonymous referees for their very fruitful and constructive comments on this manuscript.

APPENDIX

Details of the wavelet analysis

The wavelet analysis is a spectral method that allows finding dominant frequencies of the signal and their distributions in space and/or time. In principle the WT can be seen as an evolution of the windowed Fourier transform (that is a Fourier Transform done on finite size windows translated over the whole data set) by using as function basis a two parameter family of functions called *wavelets*. One of the two parameters is the translation as in the windowed Fourier transform case, and the other one is the dilatation λ (Kumar and Foufoula-Georgiou, 1994).

In the following we recall the definition of WT for a spatial series at a given latitude, $x_n = x(n\delta x)$, with equal distance spacing δx and $n = 0, \ldots, N-1$. The wavelet function will be noted as $\psi(\eta)$, depending on a non-dimensional "spatial" parameter η. In our study, we adopt the Morlet wavelet, usually used for periodic signals, which is a complex-valued, modulated Gaussian plane wave. Its expression is:

$$\psi(\eta) = \pi^{-1/4} e^{i\omega\eta} e^{-\eta^2/2} \tag{A1}$$

where ω is the nondimensional frequency.

Thus, the continuous wavelet transform of a discrete sequence x_n is defined as the convolution of x_n with a scaled and translated version of $\psi(\eta)$:

$$W_n(s) = \sum_{n'=0}^{N-1} x_{n'} \psi^* \left[\frac{(n' - n)\delta x}{s} \right] \tag{A2}$$

where the (*) indicates the complex conjugate. By varying the wavelet scale s and translating along the localized space index n, one can construct a map of $W_n(s)$ showing both the amplitude of any features versus the scale and how this amplitude varies in space (Torrence and Compo, 1998). A link between the spectral and the physical space during the wavelet analysis can be done using the following relationship, which relates the indices j of the wavelet scales ($s = s_0 2^{jdj}$) to the wavelength λ ($\lambda \approx 1{,}033.s$ – Torrence and Compo, 1998):

$$j = \frac{\ln(\lambda / 1.033 s_0)}{dj * \ln(2)} + 1 \tag{A3}$$

where $dj = 1/4$ is the spacing between discrete scales and $s_0 = 2\delta x$ the smallest scale of the wavelet. Then, the arbitrary set of wavelet scales can be interpreted as wavelengths in meters.

These concepts can be applied to the analysis of temporal time series, with obvious modifications.

Wavelet coherency and phase

The wavelet analysis, applied on two distinct data sets, allows computing other spectral products. In our study, we are interested in the coherency and phase between the chlorophyll-*a* concentrations and the SLA. To obtain these quantities, the cross-wavelet spectrum is estimated in a first step. Considering two spatial series (function of the longitude for a given time and latitude) X and Y, with wavelet transform $W_n^X(s)$ and $W_n^Y(s)$, the cross-wavelet spectrum is defined as $W_n^{XY}(s) = W_n^X(s) W_n^{Y*}(s)$, where $W_n^{Y*}(s)$ is the complex conjugate of $W_n^Y(s)$.

Then, the wavelet squared coherency is defined as:

$$R_n^2(s) = \frac{\left| \langle s^{-1} W_n^{XY}(s) \rangle \right|^2}{\langle s^{-1} |W_n^X(s)|^2 \rangle \langle s^{-1} |W_n^Y(s)|^2 \rangle} \tag{A4}$$

where $\langle . \rangle$ indicates smoothing in both space and scale. As smoothing we have used convolution with a gaussian, following Torrence and Webster (1999).

The result of (4) is between 0 and 1, and measures the cross-correlation between two spatial series as a function of the wavelength (Torrence and Webster, 1999). The wavelet-coherency phase difference between X and Y is given by:

$$\phi_n(s) = \tan^{-1}\left(\frac{\mathrm{Im}(\langle s^{-1} W_n^{XY}(s)\rangle)}{\mathrm{Re}(\langle s^{-1} W_n^{XY}(s)\rangle)}\right) \tag{A5}$$

The values obtained with the equations (A4) and (A5) allow studying the relationship between the two data sets. In our case, this method is applied to compare the spatial Rossby waves properties in SLA with those in chlorophyll-*a* concentrations.

REFERENCES

Barnier, B. 1988. A numerical study on the influence of the mid-Atlantic ridge on nonlinear first-mode baroclinic Rossby waves generated by seasonal winds. J. Phys. Oceanogr., *18*, 417-433.

Challenor, P. G., P. Cipollini and D. Cromwell. 2001. Use of the 3D Radon transform to examine the properties of oceanic Rossby waves. J. Atmos. Oceanic Tech., *18*, 1558-1566. See also: Corrigendum - 2002. J. Atmos. Oceanic Tech., *19,* 828.

Charria, G., F. Mélin, I. Dadou, M. -H. Radenac and V. Garçon. 2003. Rossby wave and ocean color: The cells uplifting hypothesis in the South Atlantic Subtropical Convergence Zone. Geophys. Res. Lett., *30(3)*, 1125, doi:10.1029/2002GL016390.

Chelton, D. B. and M. G. Schlax. 1996. Global observations of oceanic Rossby waves. Science, *272*, 234-238.

Cipollini, P., D. Cromwell, P. G. Challenor and S. Raffaglio. 2001. Rossby waves detected in global ocean color data. Geophys. Res. Lett., *28(2)*, 323-326.

Cipollini, P., D. Cromwell, M. S. Jones, G. D. Quartly and P. G. Challenor. 1997. Concurrent altimeter and infrared observations of Rossby wave propagation near 34N in the Northeast Atlantic. Geophys. Res. Lett., *24(8)*, 889-892.

Conkright, M. E., R. A. Locarnini, H. E. Garcia, T. D. O'Brien, T. P. Boyer, C. Stephens and J. I. Antonov. 2002. World Ocean Atlas 2001: Objective Analyses, Data Statistics, and Figures, CD-ROM Documentation, National Oceanographic Data Center, Silver Spring, MD, 17 pp.

Conkright, M., T. O'Brien, S. Levitus, T. P. Boyer, J. Antonov and C. Stephens. 1998. World Ocean Atlas 1998. Vol. 10, Nutrients and Chlorophyll of the Atlantic Ocean, NOAA Atlas NESDIS 36.U.S. Gov. Printing Office, Wash., D. C., 245 pp.

Cromwell, D. 2001. Sea surface height observations of the 34N 'waveguide' in the North Atlantic. Geophys. Res. Lett., *28(19)*, 3705-3708.

Dandonneau, Y., C. Menkes, T. Gorgues and G. Madec. 2004. Response to Comment on "Oceanic Rossby waves acting as a 'hay rake' for ecosystem floating by-products." Science, *304*.

Dandonneau, Y., A. Vega, H. Loisel, Y. Du Penhoat and C. Menkes. 2003. Oceanic Rossby waves acting as a "hay rake" for ecosystem floating by-products. Science, *302*, 5650.

Fu, L.-L. 2004. Latitudinal and frequency characteristics of the westward propagation of large-scale oceanic variability. J. Phys. Oceanogr., *34*, 1907-1921.

Fu, L.-L. and D. B. Chelton. 2001. Large scale ocean circulation, *in* Satellite Altimetry and Earth Sciences, L.-L. Fu and A. Cazenave, eds., Academic Press, 463 pp.

Hill, K. L., I. S. Robinson and P. Cipollini. 2000. Propagation characteristics of extratropical planetary waves observed in the ATSR global sea surface temperature record. J. Geophys. Res., *105*(C9), 21,927-21,945.

Hughes, C. W. 1996. The Antarctic Circumpolar Current as a waveguide for Rossby waves. J. Phys. Oceanogr., *26*, 1375-1387.

Kalnay, E., M. Kanamitsu, R. Kistler, W. Collins, D. Deaven, L. Gandin, M. Iredell, S. Saha, G. White, J. Woolen, Y. Zhu, M. Chelliah, W. Ebisuzaki, W. Higgins, J. Janowiak, K. C. Mo, C. Ropelewski, J. Wang, A. Leetma, R. Reynolds, R. Jenne and D. Joseph. 1996. The NCEP/NCAR 40-year reanalysis project. Bull. Amer. Meteor. Soc., *77*, 437-471.

Kawamiya, M. and A. Oschlies. 2001. Formation of a basin-scale surface chlorophyll pattern by Rossby waves. Geophys. Res. Lett., *28(21)*, 4139-4142.

Killworth, P. D. 2004. Comment on "Oceanic Rossby waves acting as a 'hay rake' for ecosystem floating by-products." Science, *304*.

Killworth, P. D. and J. R. Blundell. 2003a. Long extratropical planetary wave propagation in the presence of slowly varying mean flow and bottom topography. Part I: The local problem. J. Phys. Oceanogr., *33,* 784-801.

—— 2003b. Long extratropical planetary wave propagation in the presence of slowly varying mean flow and bottom topography. Part II: Ray propagation and comparison with observations. J. Phys. Oceanogr., *33*, 802-821.

Killworth, P. D., D. B. Chelton and R. de Szoeke. 1997. The speed of observed and theoretical long extra-tropical planetary waves. J. Phys. Oceanogr., *27*, 1946-1966.

Killworth, P. D., P. Cipollini, B. M. Uz and J. R. Blundell. 2004. Physical and biological mechanisms for planetary waves observed in sea-surface chlorophyll. J. Geophys. Res., *109*(C7), doi:10.1029/2003JC001768.

Kumar, P. and E. Foufoula-Georgiou. 1994. Wavelet analysis in geophysics: An Introduction, *in* Wavelets in Geophysics, Efi Foufoula-Georgiou and Praveen Kumar, eds., 1-43.

Le Traon, P.-Y., F. Nadal and N. Ducet. 1998. An improved mapping method of multi-satellite altimeter data. J. Atmos. Oceanic Tech., *15*, 522-534.

Longhurst, A. 1998. Ecological Geography of the Sea, Academic Press, 398 pp.

Louanchi, F. and R. G. Najjar. 2001. The mean annual cycle of nutrients and oxygen in the North Atlantic Ocean. Deep Sea Res. II, *48*, 2155-2171.

Machu, E., B. Ferret and V. Garçon. 1999. Phytoplankton pigment distribution from SeaWiFS data in the subtropical convergence zone south of Africa: A wavelet analysis. Geophys. Res. Lett., *26(10)*, 1469-1472.

Machu, E. and V. Garçon. 2001. Phytoplankton seasonal distribution from SeaWiFS data in the Agulhas Current System. J. Mar. Res., *59*, 795-812.

McClain, C. R., M. L. Cleave, G. C. Fledman, W. W. Gregg, S. B. Hooker and N. Kurig. 1998. Science quality SeaWiFS data for global biosphere research. Sea Technology, *39*, 10-16.

Mouriño, B., E. Fernandez, H. Etienne, F. Hernandez and S. Giraud. 2003. Significance of cyclonic SubTropical Oceanic Rings of Magnitude (STORM) eddies for the carbon budget of the euphotic layer in the subtropical northeast Atlantic. J. Geophys. Res., *108(C12)*, 3383, doi:10.1029/2003JC001884.

O'Reilly, J. E., S. Maritorena, B. G. Mitchell, D. A. Siegel, K. L. Carder, S. A. Garver, M. Kahru and C. McClain. 1998. Ocean color chlorophyll algorithms for SeaWiFS. J. Geophys. Res., *103(C11)*, 24,937-24,953.

Osychny, V. and P. Cornillon. 2004. Properties of Rossby waves in the North Atlantic estimated from satellite data. J. Phys. Oceanogr., *34*, 61-76.

Pingree, R. D. and B. Sinha. 1998. Dynamic topography (ERS-1/2 and Seatruth) of subtropical ring (STORM 0) in the STORM Corridor (32-34N, Eastern Basin, North Atlantic Ocean). J. Mar. Biol. Assoc. U. K., *78*, 351-376.

Polito, P. S., and P. Cornillon. 1997. Long baroclinic Rossby waves detected by TOPEX/POSEIDON. J. Geophys. Res., *102(C2)*, 3215-3235.

Polito, P. S. and W. T. Liu. 2003. Global characterization of Rossby waves at several spectral bands. J. Geophys. Res., *108(C1)*, 3018, doi:10.1029/2000JC000607.

Pottier, C., J. -P. Céron, J. Sudre, I. Dadou, S. Belamari, and V. Garçon. 2004. Dominant propagating signals in sea level anomalies in the Southern Ocean. Geophys. Res. Lett., *31*, L11305, doi:10.1029/2004GL019565.

Siegel, D. 2001. The Rossby rototiller. Nature, *409*, 76-77.

Torrence, C. and G. P. Compo. 1998. A practical guide to wavelet analysis. Bull. Amer. Meteor. Soc., *79*, 61-78.

Torrence, C. and P. J. Webster. 1999. Interdecadal Changes in the ENSO-Monsoon System. J. Climate, *12*, 2679-2690.

Uz B. M., J. A. Yoder and V. Osychny. 2001. Pumping of nutrients to ocean surface waters by the action of propagating planetary waves. Nature, *409*, 597-600.

Received: *23 September, 2004*; revised: *21 September, 2005*.